Dynamic Response of Falling Liquid Storage Container Under Transient Impact

Yang Xinglin[1], *Zhang Guilong*[1*], *Zhang Junmiao*[1], *Shao Mingyang*[2], *Cheng Dong*[2]

1. School of Energy and Power Engineering, Jiangsu University of Science and Technology, Zhenjiang 212003, P. R. China;

2. No. 713 Research Institute, China Shipbuilding Industry Corporation, Zhengzhou 450015, P. R. China

(Received 19 September 2016; revised 26 January 2018; accepted 15 October 2018)

Abstract: The dynamic response performance of a large, cylindrical, fluid-filled steel container under high-speed impact is evaluated through fluid-structure interaction analysis using arbitrary Lagrange-Eulerian (ALE) method. The ALE method is adopted to accurately calculate the structural behavior induced by the internal liquid impact of the container. The stress and strain results obtained from the finite element analysis are in line with the experimental shell impact data. The influences of drop angle, drop height, and flow impact frequency are discussed. Calculation results indicate that the impact stress and damage of the container increase with drop height. However, the amplitude of the oscillation and the impact stress increase when the container and flow impact resonance occur at a certain drop height. The impact stress shows a nonlinear relationship with drop angle.

Key words: fluid-structure interaction; impact; arbitrary Lagrange-Eulerian (ALE); nonlinear

CLC number: TB125 **Document code**: A **Article ID**: 1005-1120(2018)05-0760-10

0 Introduction

Liquid storage containers are used in many areas. The improvement of the crashworthiness of containers requires the conduct of numerous physical tests. However, these tests are expensive and complicated. On the contrary, numerical simulations can calculate and indicate deformation, stress distribution, and so on while necessitating minimal resources[1]. Therefore, improving container design and studying the dynamic response of containers are beneficial. Liquid container impact can be divided into two stages: the dynamic response and the fluid-structure interaction (FSI). Extensive research has been carried out to improve the performance of liquid containers. In recent years, the problem of liquid storage containers has attracted increasing attention[2-4]. In the 1970s, the arbitrary Lagrange-Eulerian (ALE) method was applied for the first time to calculate FSI[5-8]. Banks et al.[9] described an added-mass partitioned algorithm for solving FSI problems involving inviscid compressible fluids that interact with nonlinear solids undergoing large rotations and displacements. Elahi et al.[10] used volume of fluid method to solve the problem of two-dimensional liquid sloshing inside a container. Yu et al.[11] developed a multiphase finite element (FE) simulation method to simulate the interactions among the solid and fluid phases in an impact tank trunk. Ruiz et al.[12] developed a computationally efficient numerical model for the study of the dynamic behavior of liquid storage tanks. Musa et al.[13] used an in-house FE model to analyze the earthquake response of liquid storage containers under vertical excitations. Their results revealed the feasibility of estimating the capacities of a number of steel conical tanks. Chen et al.[14] studied the sloshing of stratified liquid with density in a three-dimensional cylindrical tank. Instead of using velocity potential for uni-

* Corresponding author, E-mail address: 394779460@qq.com.

How to cite this article: Yang Xinglin, Zhang Guilong, Zhang Junmiao, et al. Dynamic response of falling liquid storage container under transient impact[J]. Trans. Nanjing Univ. Aero. Astro., 2018,35(5):760-769.
http://dx.doi.org/10.16356/j.1005-1120.2018.05.760

form liquid, they adopted governing equations and boundary conditions in terms of a pressure function and a density function. New frequencies made the motion history of the free surface irregular. Yu et al.[15] studied the free surface oscillation of the liquid inside elastic containers on the basis of a mixed Eulerian-Lagrange approach. Although the ALE method has been proven effective for FSI problems, some researchers doubt its efficiency because of its computational intensity[16]. The response of shield buildings under seismic loading was studied by Lu et al.[17], who found that the analysis of FSI could improve the design of liquid storage tanks. Ren et al.[18] studied the interaction between a structure undergoing large deformation and the fluid.

1 Finite Element Discretization

1.1 ALE method

In the ALE description, the mass equation can be described as

$$\frac{\partial \rho(\chi,t)}{\partial t}+\rho\frac{\partial u_i}{\partial x_i}+c_i\frac{\partial \rho}{\partial x_i}=0 \tag{1}$$

where χ is the ALE coordinate, x the Eulerian coordinate, and ρ the fluid density. c_i is the ALE relative velocity, $c_i=u_i-v_i$, here v_i is the velocity of the referential coordinate and u_i the velocity of the material.

The motion equation is

$$\rho\frac{\partial u_i(\chi,t)}{\partial t}+\rho c_j\frac{\partial u_i}{\partial x_i}=\frac{\partial \sigma_{ij}}{\partial x_i}+\rho b_i \tag{2}$$

where b_i is the unit body force.

The constitutive relation of Newtonian fluids and the strain-velocity relation are introduced as

$$\sigma_{ij}=-p\delta_{ij}+\mu\left(\frac{\partial u_i}{\partial x_j}+\frac{\partial u_j}{\partial x_i}\right) \tag{3}$$

where μ is the kinematic viscosity. Natural and essential boundary conditions are imposed on the boundary.

In this work, the constitutive equation of the fluid is composed of the equation of state and the material model. The equation of state defines the volumetric compression behavior of the fluid, and the material model defines the relationship between the shear stress and the shear strain rate.

1.2 Fluid structure interaction

The approach used in this work to solve the FSI problem is apenalty-based FE method with an ALE description.

The gas-to-liquid interface can be modeled with no separation and no slip contact, that is, the two materials are firmly attached together along their interface. Alternatively, the two materials can share common nodes along their interface to achieve the same modeling effect while avoiding contact definition. By contrast, the gas-to-liquid contact definition performs well when the entire container structure is modeled with solid elements. The "shared nodes" strategy results in a relatively stable contact performance.

Container deformation can be described as

$$\rho_s\left.\frac{\partial^2 u}{\partial t^2}\right|_X=\frac{\partial \sigma_{ij}}{\partial x_i}+f_i \tag{4}$$

where X denotes the Lagrange coordinate, ρ_s the density of the structure, f_i the body force, and u the displacement of the structure.

Eqs. (1)(2)(4) are coupled under the following geometric compatibility and mechanical equilibrium conditions that should be satisfied on the FSI interfaces.

$$v=\left.\frac{\partial u}{\partial t}\right|_X \tag{5}$$

$$F_f+F_s=0 \tag{6}$$

where F_f and F_s are the interaction forces acting on the FSI interfaces.

The penalty function method is employed to process solid boundary and fluid boundary. This method can promote energy conservation during the coupling process. The standard projection method consists of two steps: a predictor step and a corrector one. In the predictor step, an auxiliary discrete velocity, which does not satisfy the divergence-free condition, is computed. In the corrector step, an iterative correction is introduced to enforce the incompressibility constraint. This projection allows us to solve the pressure and velocity field separately, although it does not recover the original boundary conditions on pressure, which are defined implicitly in the original momentum equation[19]. The coupling force calculat-

ed on the basis of the penalty function is

$$F_s = \frac{d^2 Z}{dt^2} + \xi_i \frac{dZ}{dt} + \frac{m_s + m_f}{m_s - m_f} \frac{\alpha K_i A_i^2}{V_i} Z \quad (7)$$

where ξ_i is the damping coefficient, m_s the solid mass, m_f the fluid mass, α the scaling of quality, and A_i, V_i, and K_i denote the unit area, unit volume, and element capacity, respectively.

2 Model

2.1 Experimental procedure

An experiment was conducted to investigate the dynamic response of a cylindrical container under impact conditions. The diameter and height of the container were 2.2 m and 7 m, respectively. The thickness of the container was 30 mm. It held 70% water to its capacity (in volume). In the experiment, the container was dropped onto a concrete surface by activating the quick-release mechanism at a height of 20 m.

The experimental setup is shown in Fig. 1. Pressure transducers were instrumented to measure the stress of the container. During the experiment, the bottom and shoulder exhibited significant deformation. Therefore, the bottom and shoulder required attention in the dynamic simulation. A pressure transducer was added at position 2 to obtain a detailed understanding of the dynamic response of the container.

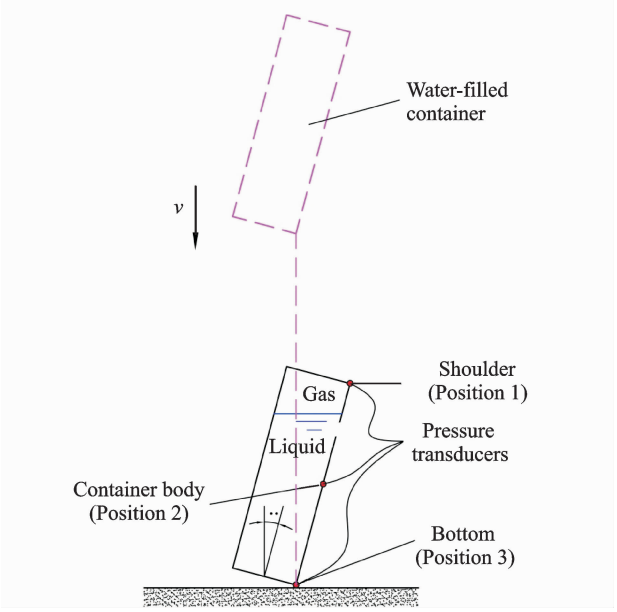

Fig. 1 Sketch map of experimental apparatus

2.2 Numerical procedure

Belytschko-Tsay shell elements with four nodes were used to discretize the container and floor. Exactly 5 860 quadrilateral shell elements were divided between the container and the floor. The FE model is shown in Fig. 2, and the floor is assumed to be rigid.

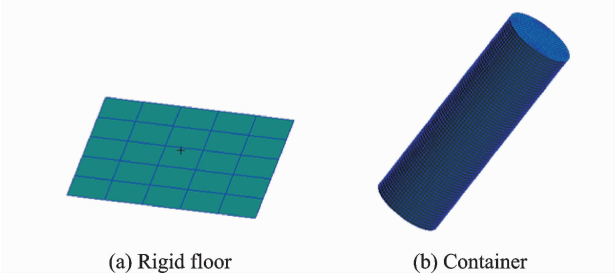

Fig. 2 FE models

When a container is not fully filled with water, a significant amount of air exists above the water level, as shown in Fig. 3. Owing to the excessively large deformations of the fluid inside a tank, a pure Lagrange description may not be an appropriate option. Hence, a multi-material ALE formulation with a second-order accurate advection method was chosen for the treatment of the fluid in this study. "Multi-material" means that each element of the mesh can contain two or more materials, such as water and air in this case. The ALE formulation allows the motion of the mesh to be independent of the material flow without causing distortion problems[20]. The fluid inside the box (water and air) is discretized with eight-node solid hexahedron elements with an ALE formulation. The total number of the elements and nodes of the whole system are 42,112 and 43,814, respectively.

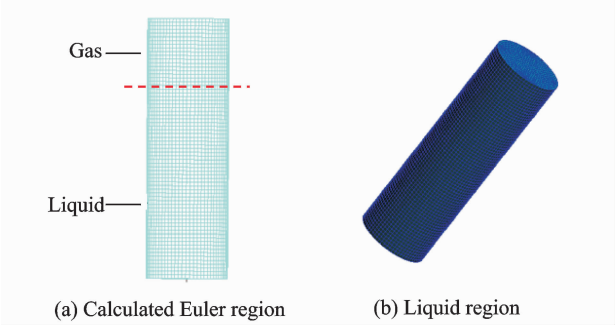

Fig. 3 FE model of Euler domain

The present investigation is focused on large container and simple container designs. In the experiment, the drop height is H, the thickness of the container is Th, and thus, the impact speed is v ($v=\sqrt{2gh}$). The drop angle is θ. A schematic of such a cylinder container, which was supplied by a national defense experiment, is given in Fig. 4, which shows the main characteristics, drop angle θ, and dimensions.

The parameters of the steel, liquid, and gas materials are summarized in Table 1. The liquid parameters were based on the properties of water, and the gas parameters were based on the properties of air. The coefficient of friction was assumed to be 0.6 for steel-on-steel contact and 0.3 for the contact between the container and the rigid floor[21].

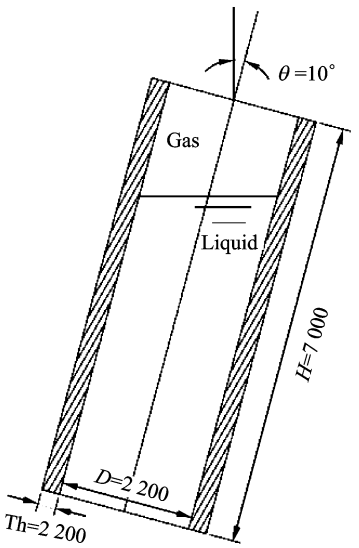

Fig. 4 Sketch map of cylinder container and geometrical data

Table 1 Material properties

Gas		Water		Container	
Density/(kg · m^{-3})	1.29	Density/(kg · m^{-3})	1 000	Density/(kg · m^{-3})	7 850
Specific internal energy/ (J · kg^{-1})	83 950	Specific internal energy/ (J · kg^{-1})	211 041	Young's modulus / GPa	206
Specific heat ratio	1.4	Bulk modulus / MPa	2 200	Poisson's ratio	0.3
				Yield stress / MPa	420
				Fracture strain	0.3

The contact between the container surface and the rigid floor surface was defined, and the FSI between the container and the Euler domain was established. Under impact conditions, both domains showed an initial speed V, which corresponded to the drop height H. The drop angle was defined as θ to make the results of the FE model and theoretical predictions comparable.

3 Results and Discussion

3.1 Comparison of experimental and numerical results

In this section, the results of numerical simulation are compared with those of the physical test. Fig. 5(a) shows the principal stress curves of the shoulder, body, and bottom of the container. During impact, the bottom was the first to come into contact with the floor. Thus, its stress reached the peak value of 550.2 MPa.

The slope of the trace represents the stress rise rate. When the shoulder touched the floor, the water moved with it. Thus, the shoulder stress reached 443 MPa. The maximum stress of the container body was 178 MPa. Fig. 5(b) displays the deformation of the container. Only the shoulder and the bottom exhibited plastic deformation during impact.

Fig. 6 shows the comparison of stresses at Position 3. The stress curves exhibited characteristics of strong nonlinear oscillations. The stress increased dramatically from zero to the maximum. Then, the stress decreased, and Position 1 touched the floor. The numerical simulation and experiment showed a good agreement.

3.2 Dynamic response analysis

As a result of the limitations of laboratory apparatus, carrying out additional experiments under different conditions is difficult. On the con-

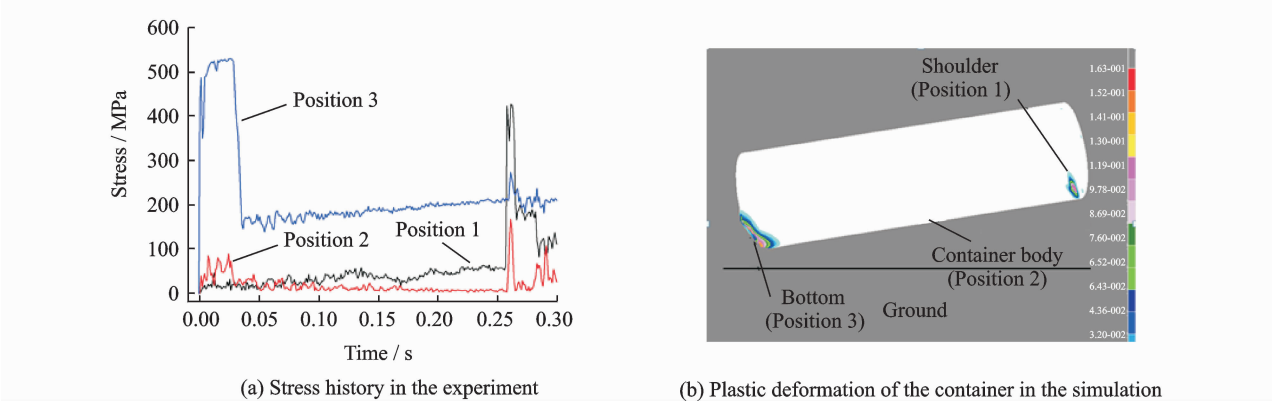

(a) Stress history in the experiment (b) Plastic deformation of the container in the simulation

Fig. 5 Stress and deformation of the model

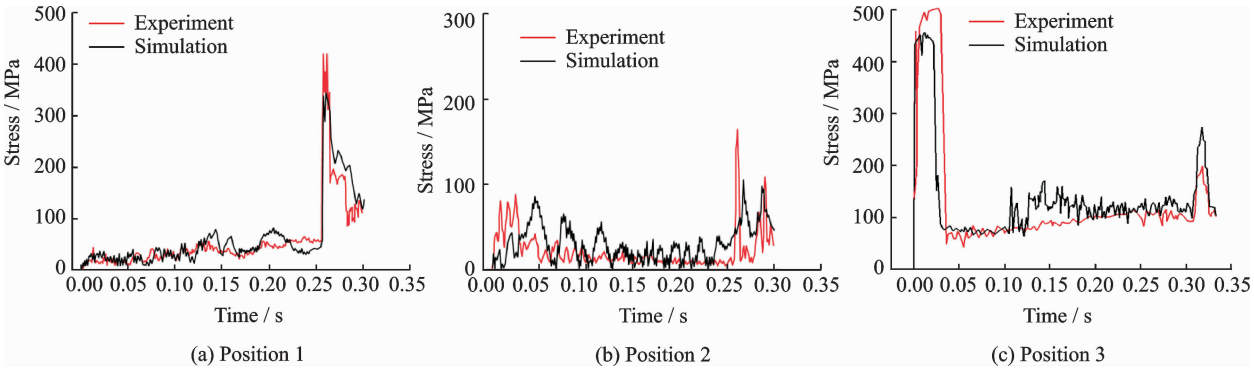

(a) Position 1 (b) Position 2 (c) Position 3

Fig. 6 Comparison of experimental and simulation stress histories of the bottom of the container

trary, numerical simulations can easily accomplish these works. Moreover, numerical simulations can facilitate the investigation and analysis of the results. The dynamic responses of the container were simulated and analyzed in two aspects: drop angles and drop heights.

3.2.1 Drop angle

Eight simulation tests were performed according to different drop angles (10°, 20°, 30°, 40°, 50°, 60°, 70°, and 80°) to examine the effect of drop angles. In these tests, the containers held the same amount of water (70%), and all the drop heights equalled to 10 m.

Fig. 7 shows the maximum stresses of the bottom of the container under different drop angles. The stresses under drop angles of 20°, 30°, and 40° were larger than those under other drop angles. This result is explained as follows. When the angle was 10°, most of the water impact force and gravitational force acted on the container bottom. The container bottom under such condition absorbed greater energy than it did under other

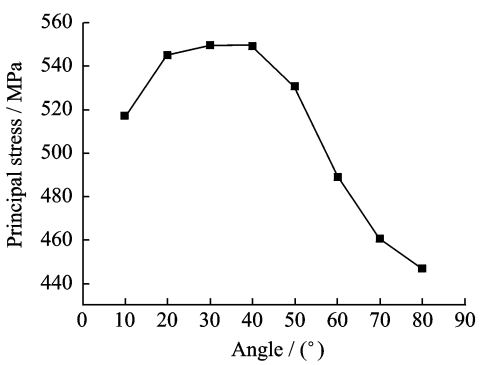

Fig. 7 Maximum stresses of the container at different angles

conditions; thus, its maximum stress was smaller.

Fig. 8 presents the stress histories of Position 4, which lies on the axis of the symmetry of the container around Position 3. When the drop angle was less than 40°, the stress of Position 4 was larger than that under other drop angles. Therefore, the impact force on the bottom of the container increased with the decrease of the drop angle. When the drop angle was greater than 50°,

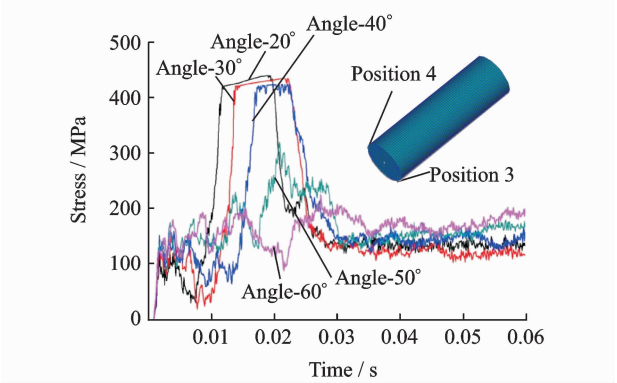

Fig. 8 Stress histories of Position 4 at different angles

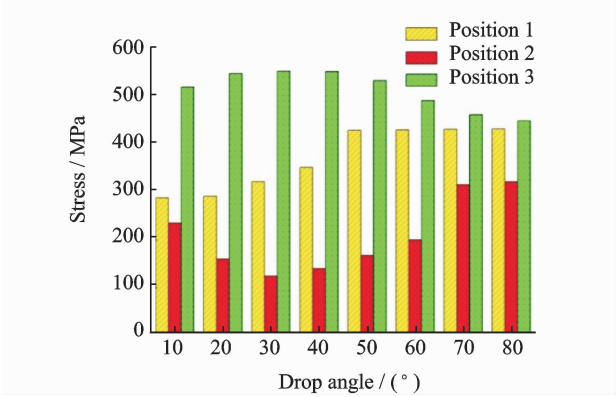

Fig. 10 Maximum stresses at different angles

the stress of Position 3 decreased.

Fig. 9 compares the kinetic energy histories of the container under different drop angles. The container bounced after impact. The kinetic energy increased with the rise of the drop angle. At the drop angle of 70°, the impact time was the shortest. Thus, the maximum stress of Position 3 decreased as the drop angle increased. In particular, when the drop angle was less than 40°, the maximum stress of Position 3 showed no obvious decrease.

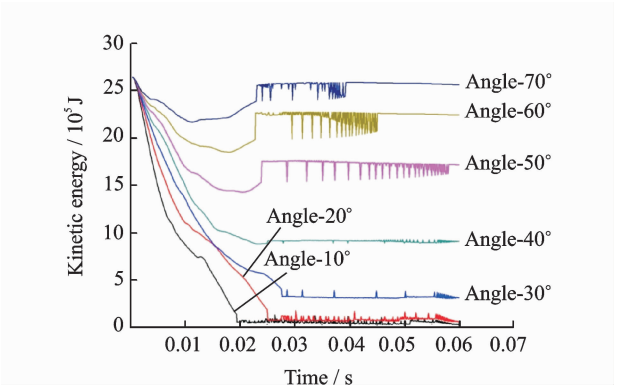

Fig. 9 Kinetic energy histories of the container at different angles

Fig. 10 displays the maximum stresses of the three positions under different drop angles. In all simulations, the stress of Position 3 was always the highest. In addition, the stress of Position 1 was over 300 MPa when the shoulder touched the ground. The stress of Position 1 increased with the rise of the top angle. At the 50° angle, the stress of Position 1 even reached 427 MPa. Therefore, Position 1 became another frangible area, in addition to Position 3, as the drop angle increased.

3.2.2 Drop height

This research also investigates the influence of drop height on the container. In the simulations, all the drop angles equalled to 50°, and the containers held the same amount of water(70%). The drop heights were 10, 20, 30, 40, 50, 60, and 70 m.

Fig. 11 presents the stress histories of the bottom of the container (Position 3) for two drop heights. The patterns and periods of the main oscillation showed obvious similarities. The maximum stress of Position 3 at a 50 m drop height was larger than the maximum stress at a 40 m drop height. During impact, the stress increased rapidly. Thereafter, the container showed plastic deformation, the contact point showed depression characteristics, and the principle stress decreased. A portion near the contact point impinged on the ground, and the stress increased again. As the container bounced after the impact, the stress decreased rapidly. The container wall continued to oscillate. During impact, the water

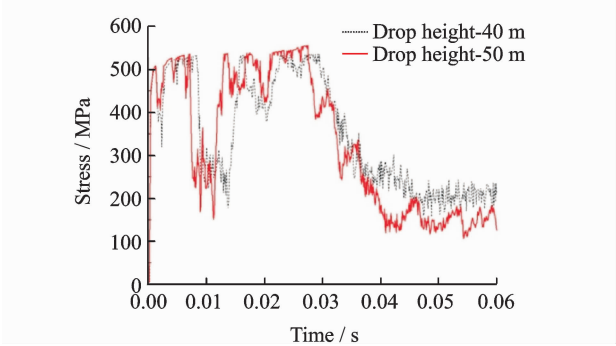

Fig. 11 Stress histories of Position 3 at different heights

away from the wall did not indicate wall deformation, and waves traveled at high speeds, thus producing high frequencies.

Fig. 12 shows the simulated water flow in the fluid domain when the water reached the top of the container at different drop heights. During impact, the fluid away from the wall did not indicate wall movement, and the waves started to travel at the unconfined speed of 1 485 m/s ($\sqrt{K/\rho}$), thus producing pressure magnitudes of 20.9, 29.7, 36.2, and 41.9 MPa, which corresponded to drop heights of 10, 20, 30, and 40 m. By contrast, the fluid particles next to the container wall started to move radially outward because of the deformation of the wall. This fluid movement radiateda radial decompression wave toward the bottle axis. The pressure at the bottom continued to oscillate as a result of the radial waves. At the same time, the large deformation absorbed a high amount of impact energy. In addition, some superimposed pressure oscillations traveling in different directions were observed in the system immediately after impact. The value of flow impact force showed minimal effect on the container, but the flow could resonate with the container. The impact frequency showed a significant impact on the dynamic response of the container.

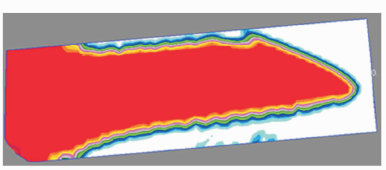

(a) Drop height-10 m

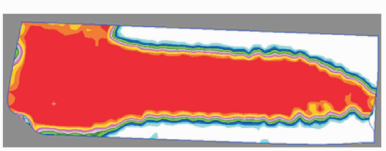

(b) Drop height-20 m

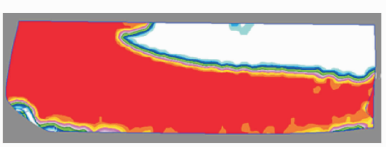

(c) Drop height-30 m

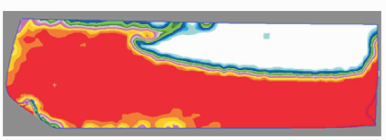

(d) Drop height-40 m

Fig. 12 Water flow at 0.2 s at different altitudes

Fig. 13 compares the stress histories of Positions 1 and 2 under different drop heights. The maximum stresses of Positions 1 and 2 at a 40 m drop height were larger than the maximum stresses at a 50 m drop height; the amplitude of oscillations were also higher in the former than in the latter. This result can be attributed to the natural oscillating frequency of the container, which was close to the flow impact frequency at a 40 m drop height. The natural frequency was 0.332 Hz, and the frequencies of Positions 1 and 2 at 50 and 40 m drop heights were 0.213 and 0.319 Hz, respectively, as shown in Fig. 14. Positions 1 and 2 showed minimal deformation upon impact; therefore, the natural frequency remained unchanged.

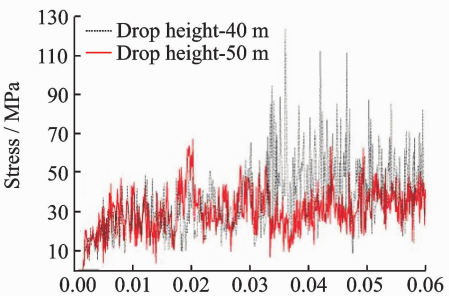

(a) Position 1

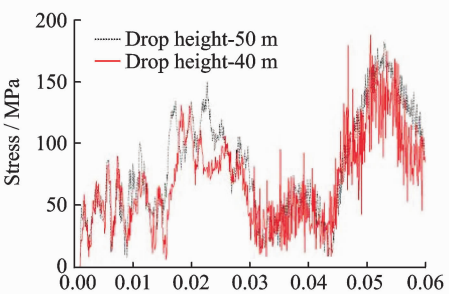

(b) Position 2

Fig. 13 Stress histories of Positions 1 and 2 at different altitudes

Fig. 15 compares the maximum stresses of three positions under different drop heights. At 40 m and 50 m drop heights, the stress of Position 2 was nearly equal to the stress of Position 1.

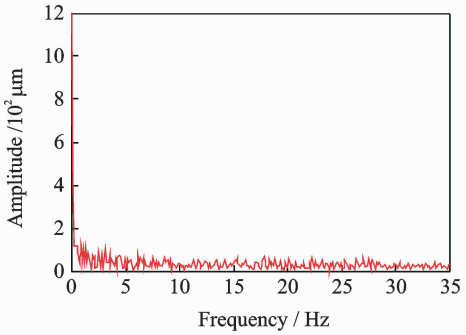

(a) Frequency of Position 1 at 40 m drop height

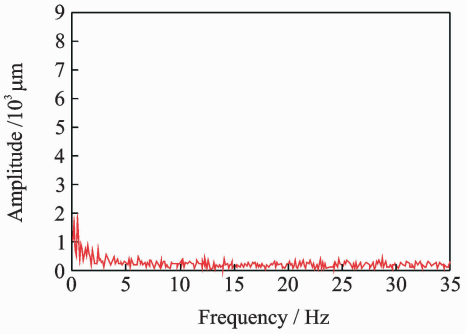

(b) Frequency of Position 1 at 50 m drop height

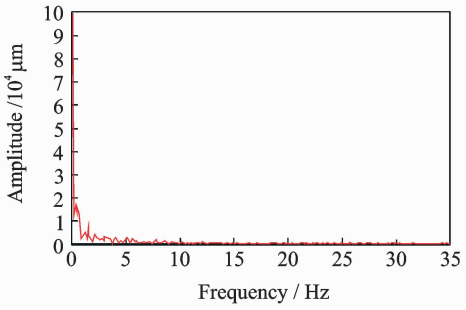

(c) Frequency of Position 2 at 40 m drop height

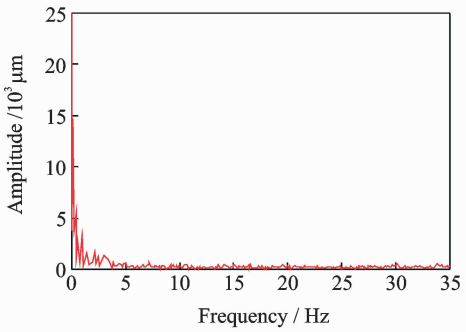

(d) Frequency of Position 2 at 50 m drop height

Fig. 14 Frequency of positions 1 and 2 at different altitudes

Therefore, Position 2 became another frangible area with the increase of the drop height. The maximum stresses of Positions 1 and 3 increased slowly.

Based on the above analysis, we can find that

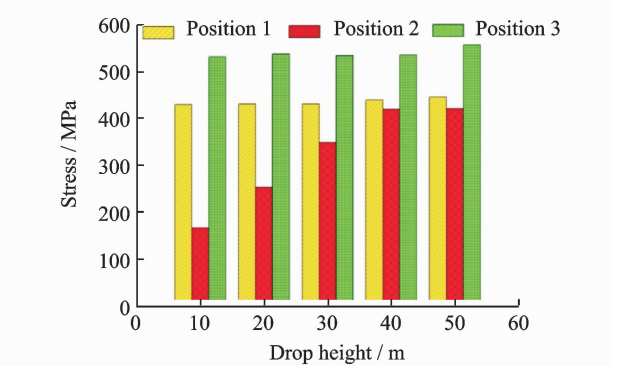

Fig. 15 Maximum stresses at different altitudes

the larger the angle, the lower the height, the smaller the stress of the tank. Therefore, when designing the tank, the radius of the contour Fillet of the tank bottom and the thickness of the tank should be as large as possible. In future research, we can analyze the other factors, such as liquid storage, and give more design suggestions.

4 Conclusions

Experiment results and numerical simulation tests were analyzed to thoroughly understand the dynamic response of fluid-filled containers upon impact. Some conclusions are summarized as follows:

(1) The results of the multi-material ALE method were in line with the experimental findings. The multi-material ALE method was found to be an effective method for predicting the dynamic response of fluid-filled containers.

(2) The drop angle exerted a significant effect on container crashworthiness. According to the experiment and simulation results, the bottom of the container was a frangible position. When the drop angle was greater than 50°, the shoulder became another frangible position.

(3) The study of the effect of drop height revealed that the maximum stress magnitude increased with the increase of drop height. The water flow impact frequencies were not the same at different drop heights. When the drop height was 40m, the natural oscillating frequency of the container was close to the flow impact frequency. The amplitude of the oscillation and impact stres-

ses of Positions 1 and 2 increased substantially.

In summary, the multi-material ALE method combined with numerical simulation can effectively analyze the dynamic response of a falling liquid storage container under transient impact. The analysis results can meet the engineering requirements.

Acknowledgement

This work was supported by the Prospective Joint Research Fund of the Jiangsu Provincial Department of Science and Technology Agency(No. BY2016073-11).

References:

[1] CAO Yuan, JIN Xianlong. Dynamic response of flexible container during the impact with the ground [J]. International Journal of Impact Engineering, 2010, 37:235-254.

[2] ANGHILERI M, CASTELLETTI L M L, TIRELLI M. Fluid-structure interaction of water filled tanks during the impact with the ground[J]. International Journal of Impact Engineering, 2005, 31(3): 235-254.

[3] CAI Liguang, AL-OSTAZ A, LI X, et al. Protection of steel railcar tank containing liquid chlorine from high speed impact by using polyhedral oligomeric silsesquioxane-enhanced polyurea [J]. International Journal of Impact Engineering, 2014, 75:1-10.

[4] HIRT C W, AMSDEN A A, COOK J L. An arbitrary Lagrange-Eulerian computing method for all flow speeds[J]. Journal of Computational Physics, 1974, 14:227-53.

[5] LEE C S, CHO J R, LIM W S, et al. Evaluation of sloshing resistance performance for LNG carrier insulation system based on fluid-structure interaction analysis [J]. Ocean Engineering, 2013, 5:1-20.

[6] HAY A, ETIENNE S, GARON A, et al. Time-integration for ALE simulations of fluid-structure interaction problems: Step size and order selection based on the BDF [J]. Computer Methods in Applied Mechanics and Engineering, 2015, 295:172-195.

[7] MANDAL K K, MAITY D. Nonlinear finite element analysis of elastic water storage tanks [J]. Engineering Structures, 2015, 99:666-676.

[8] FARHAT C, LAKSHMINARAYAN V K. An ALE formulation of embedded boundary methods for tracking boundary layers in turbulent fluid-structure interaction problems [J]. Journal of Computational Physics, 2014, 263(C):53-70.

[9] BANKS J W, HENSHAW W D, KAPILA A K, et al. An added-mass partition algorithm for fluid-structure interactions of compressible fluids and nonlinear solids [J]. Journal of Computational Physics, 2016, 305(C):1037-1064.

[10] ELAHI R, PASSANDIDEH-FARD M, JAVANSHIR A. Simulation of liquid sloshing in 2D containers using the volume of fluid method[J]. Ocean Engineering, 2015, 96:226-244.

[11] YU H, JEONG D Y. Impact dynamics and puncture failure of pressurized tank cars with fluid-structure interaction: A multiphase modeling approac[J]. International Journal of Impact Engineering, 2015, 90: 12-25.

[12] RUIZ R O, LOPEZ-GARCIA D, TAFLANIDIS A A. An efficient computational procedure for the dynamic analysis of liquid storage tanks[J]. Engineering Structures, 2015, 85:206-218.

[13] MUSA A, DAMATTY A A E. Capacity of liquid-filled steel conical tanks under vertical excitation[J]. Thin-Walled Structures, 2016, 103:199-210.

[14] CHEN J Z, KIANOUSH M R. Generalized SDOF system for seismic analysis of concrete rectangular liquid storage tanks [J]. Engineering Structures, 2009, 31:2426-2435.

[15] YU Hailing, FAN Jiangwen. Foliar carbon, nitrogen, and phosphorus stoichiometry in a grassland ecosystem along the Chinese grassland transect[J]. Acta Ecologica Sinica, 2017, 37:133-139.

[16] FRANCI A, ONATE E, CARBONELL J M. Unified Lagrange formulation for solid and fluid mechanics and FSI problems[J]. Computer Methods in Applied Mechanics and Engineering, 2016, 298: 520-547.

[17] LU D, LIU Y, ZENG X. Experimental and numerical study of dynamic response of elevated water tank of AP1000 PCCWST considering FSI effect[J]. Annals of Nuclear Energy, 2015, 81:73-83.

[18] REN Y T, QIU X M, YU T X. Verification of a theoretical model of tensor skin under water impact by considering the fluid-structure interaction[J]. International Journal of Impact Engineering, 2016, 92: 66-74.

[19] CERRONI D, MANSERVISI S. A penalty-projection algorithm for a monolithic fluid-structure interaction solver[J]. Journal of Computational Physics, 2016, 313:13-30.

[20] ARRAYAGO I, REAL E, GARDNER L. Description of stress-strain curves for stainless steel alloys

[J]. Materials and Design, 2015, 87:540-552.

[21] LI K, WANG Z, TANG W, et al. Experimental and numerical analysis of laterally impacted stiffened-plates considering the effect of strain rate[J]. Ocean Engineering, 2015, 99:44-54.

Dr. **Yang Xinglin** received his M. S. degree in Internal Combustion Engine from Harbin Institute of Marine Engineering in 1989. In 2005, he received the Ph. D. degree in Mechanical and Electrical Engineering from Nanjing University of Aeronautics and Astronautics(NUAA). His research interests are marine turbine system integration and performance optimization.

Mr. **Zhang Guilong** received his B. S. degree in Thermal and Power Engineering and M. S. degree in Marine Engineering from Jiangsu University of Science and Technology in 2012 and 2017, respectively. His research interests include fluid-solid coupling and structural mechanics.

Dr. **Zhang Junmiao** received his M. S. degree in Mechanical Engineering from the School of Mechanical Engineering of Jiangsu University of Science and Technology in 2008. In 2013, he received the Ph. D. degree in Mechanical Design and Theory from the School of Aeronautics and Astronautics, NUAA. His research interests are focused on mechanical structural strength.

Mr. **Shao Mingyang** received his B. S. degree in Energy and Power Engineering from the School of Mechanical and Electrical Engineering of the Texas College in 2012. His research interests are focused on the fatigue life of steam turbine rotors.

Mr. **Cheng Dong** is an engineer at the 713 Institute of China Shipbuilding Industry Corporation.

(Production Editor: Wang Jing)